MINERALOGICAL CHARACTERIZATION OF SANDSTONE AND CLAY, NORTH-EAST CONSTANTINE.

Submited on 08/03/2014 – Accepted on 19/12/2015

Abstract

The north-east area of Constantine has a very complex geological setting. The variety of sedimentary rocks such as sandstone and clay in abundance, represent a big importance in the industry and road infrastructure.
The X-ray diffraction (XRD) analysis, Scanning Electron Microscopy SEM/EDS, FTIR spectroscopy of sandstone and clay are required for qualitative and quantitative analysis of the existing phases.
In addition, chemical analysis of the same samples is required to confirm the XRD, EDS (Energy Dispersive X ray Spectroscopy) and FTIR spectroscopy results.
The results of this multidisciplinary study, obtained by various analytical techniques, show a good agreement on the existing phases.

Keywords: *Sandstone, Clay, XRD, SEM/EDS, FTIR*

M BENYAMINA
L CHETIBI
M BOUCHEAR

Materials Sciences and Applications Research Unit, Department of Physics, Faculty of Exact Sciences, Frères Mentouri University, Constantine, Algeria.

NOMENCLATURE

a	Defined constant in the elliptic coordinates, (distance to the poles).	(m)
c_p	Specific heat at constant pressure.	($J.kg^{-1}.K^{-1}$)
e_1	Eccentricity of the internal ellipse.	
Fr	Geometrical factor of form	
$\vec{g}$	Gravitational acceleration.	($m.s^{-2}$)
Gr	Grashof number defined by $Gr = \frac{g\beta a^3}{\upsilon^2}\Delta T$.	
h	Dimensional metric coefficient.	(m)
H	Dimensionless metric coefficient.	
Nu	Local Nusselt number.	
$\overline{Nu}$	Average Nusselt number.	
P	Stress tensor.	
Pr	Prandtl number defined by $\Pr = \frac{\nu \rho c_p}{\lambda}$.	
S_Φ	Source term.	
T	Fluid's temperature.	(K)
T_1	Hot wall temperature.	(K)
T_2	Cold wall temperature.	(K)
ΔT	Temperature deference.$\Delta T=T_1-T_2$.	(K)
V_η, V_θ	Velocity components according to η and θ.	($m.s^{-1}$)
$\vec{V}$	Velocity vector.	($m.s^{-1}$)

Greek letters

α	Inclination angle.	(°)
β	Thermal expansion coefficient.	(K^{-1})
Γ_φ	Diffusion coefficient.	
λ	Thermal conductivity of the fluid.	($W.m^{-1}.K^{-1}$)
υ	kinematic viscosity.	($m^2.s^{-1}$)
ρ	Density.	($kg.m^{-3}$)
η ,θ, z	Elliptic coordinates.	
ψ	function of current.	($m^2.s^{-1}$)
ω	vorticity.	(s^{-1})
φ	General function.	

Superscripts

+	dimensionless parameters.

Subscripts

i	Inner.
e	Outer.
éq	Equivalent
Ni	Points number along the coordinate η
NN	Points number along the coordinate θ
η	According to the coordinate η
θ	According to the coordinate θ

1. INTRODUCTION

The study of heat transfer by natural convection, in the annular spaces formed by elliptic cylinders with horizontal axes centered or eccentric, has given rise to many works include such as Zhu et al. (2004) who have made a numerical study into the annulus between two centered elliptic cylinders, using D.Q method (Differential Quadrature) to solve their equations. Djezzar el al. (2004), (2005) and (2006) mean while, have studied numerically natural convection in an annulus formed by two elliptical cylinders and horizontal axes confocal using the formulation in primitive variables, they could detect multi-cellular flows when Grashof number increases, for certain geometries, and for the three parietal thermal conditions used.

© Frères Mentouri University, Constantine, Algeria, 2018.

In this work we propose a numerical simulation using the finite-volume method described by Patankar (1980), the elliptic coordinates cited by Moon (1961) and the vorticity stream-function formulation illustrated by Nogotov (1978) to solve the equations governing the phenomenon studied. The mesh adopted for the execution of our calculations is (101x111).

2. Theoretical analysis

We consider an annular space, filled with a Newtonian fluid (in this case air), located between two elliptical cylinders, and two horizontal and centered diametrical planes. Figure 1 represents a cross-section of the system.

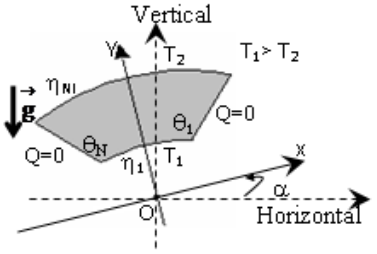

FIG. 1 Cross-section of the system

Both lower and upper walls are elliptical, isothermal and respectively maintained at temperatures T_1 and T_2 with $T_1>T_2$. The two diametrical plans are adiabatic.

It occurs in the enclosure natural convection that we propose to study numerically.

We consider an incompressible fluid flow, two dimensional, permanent and laminar with constant physical properties and we use the approximation of Boussinesq which considers the variations of the density ρ negligible at all terms of the momentum equations except in the term of gravity whose variations with temperature supposed linear, generate the natural convection.

Viscous dissipation and the work of pressure forces are negligible in the heat equation; the radiation is not considered.

With these assumptions the equations governing our problem can be written in vectorial form as follows:

- Continuity equation:

$$\mathrm{div}\,\vec{V} = 0 \tag{1}$$

- Momentum equation:

$$(\vec{V}.\vec{\mathrm{grad}})\vec{V} = \frac{\rho}{\rho_0}\vec{g} + \frac{\nabla P}{\rho_0} \tag{2}$$

- Heat equation:

$$(\vec{V}.\vec{\mathrm{grad}})T = \frac{\lambda}{\rho c_p}\nabla^2 T \tag{3}$$

It is convenient to define a reference frame such as the limits of the system result in constant values of the coordinates. The coordinates known as "elliptic" (η,θ) allow, precisely in our case to obtain this result. Thus the two elliptic isothermal walls will be represented by η_1 and η_{NI} and the two adiabatic walls will be represented by θ_1 and θ_{NN}. The transition from Cartesian coordinates to elliptic coordinates is done using the following relations:

$$\left.\begin{aligned} x &= a.ch(\eta).\cos(\theta) \\ y &= a.sh(\eta).\sin(\theta) \end{aligned}\right\}$$

The equations (1), (2) and (3) are written respectively:

$$\frac{\partial}{\partial\eta}(h V_\eta) + \frac{\partial}{\partial\theta}(h V_\theta) = 0 \tag{5}$$

$$\frac{V_\eta}{h}\frac{\partial\omega}{\partial\eta} + \frac{V_\theta}{h}\frac{\partial\omega}{\partial\theta} =$$

$$\frac{g\beta}{h}\left\{\begin{aligned} &[F(\eta,\theta)\cos(\alpha) - G(\eta,\theta)\sin(\alpha)]\frac{\partial T}{\partial\eta} \\ &-[F(\eta,\theta)\sin(\alpha) + G(\eta,\theta)\cos(\alpha) +]\frac{\partial T}{\partial\theta} \end{aligned}\right\}$$

$$+\frac{\nu}{h^2}\left(\frac{\partial^2\omega}{\partial\eta^2} + \frac{\partial^2\omega}{\partial\theta^2}\right) \tag{6}$$

$$V_\eta\frac{\partial T}{\partial\eta} + V_\theta\frac{\partial T}{\partial\theta} = \frac{\lambda}{\rho c_p}\frac{1}{h}\left(\frac{\partial^2 T}{\partial\eta^2} + \frac{\partial^2 T}{\partial\theta^2}\right) \tag{7}$$

With the introduction of vorticity defined by:

$$\omega = -\frac{1}{h^2}\left(\frac{\partial^2\psi}{\partial\eta^2} + \frac{\partial^2\psi}{\partial\theta^2}\right) \tag{8}$$

After the introduction of the stream-function, in order to check the continuity equation identically.

$$\left.\begin{aligned} h &= a\left(sh^2(\eta) + \sin^2(\theta)\right)^{1/2} \\ F(\eta,\theta) &= \frac{sh(\eta)\cos(\theta)}{\left(sh^2(\eta) + \sin^2(\theta)\right)^{1/2}} \\ G(\eta,\theta) &= \frac{ch(\eta)\sin(\theta)}{\left(sh^2(\eta) + \sin^2(\theta)\right)^{1/2}} \end{aligned}\right\} \tag{9}$$

By posing the following adimensional quantities:

D_h= a (arbitrarily selected focal distance)

$$H = \frac{h}{D_h},\quad V_\eta^+ = V_\eta\frac{D_h}{\nu},\quad V_\theta^+ = V_\theta\frac{D_h}{\nu},\quad \omega^+ = \omega\frac{D_h^2}{\nu},$$
$$\psi^+ = \frac{\psi}{\nu} \text{ and } T^+ = \frac{T - T_2}{T_1 - T_2}$$

The equations (5), (6), (7) and (8) becomes:

$$\frac{\partial}{\partial\eta}(H V_\eta^+) + \frac{\partial}{\partial\theta}(H V_\theta^+) = 0 \tag{10}$$

$$\frac{V_\eta^+}{H}\frac{\partial \omega^+}{\partial \eta}+\frac{V_\theta^+}{H}\frac{\partial \omega^+}{\partial \theta}=$$

$$\frac{Gr}{H}\left\{\begin{array}{l}\left[F(\eta,\theta)\cos(\alpha)-G(\eta,\theta)\sin(\alpha)\right]\frac{\partial T^+}{\partial \eta}\\ -\left[\mathrm{F}(\eta,\theta)\sin(\alpha)+G(\eta,\theta)\cos(\alpha)+\right]\frac{\partial T^+}{\partial \theta}\end{array}\right\}$$

$$+\frac{1}{\mathrm{H}^2}\left(\frac{\partial^2 \omega^+}{\partial \eta^2}+\frac{\partial^2 \omega^+}{\partial \theta^2}\right) \qquad (11)$$

$$HV_\eta^+\frac{\partial \mathrm{T}^+}{\partial \eta}+\mathrm{H}V_\theta^+\frac{\partial \mathrm{T}^+}{\partial \theta}=\frac{1}{\mathrm{P_r}}\left(\frac{\partial^2 \mathrm{T}^+}{\partial \eta^2}+\frac{\partial^2 \mathrm{T}^+}{\partial \theta^2}\right) \qquad (12)$$

$$\omega^+=-\frac{1}{H^2}\left[\frac{\partial^2 \psi^+}{\partial \eta^2}+\frac{\partial^2 \psi^+}{\partial \theta^2}\right] \qquad (13)$$

The boundary conditions are: For the elliptical hot wall ($\eta = \eta_1$= constant) we have:

$V_\eta^+ = V_\theta^+ = \frac{\partial \psi^+}{\partial \theta} = \frac{\partial \psi^+}{\partial \eta} = 0$, $T_1^+ = 1$ and

$\omega^+=-\frac{1}{H^2}\left[\frac{\partial^2 \psi^+}{\partial \eta^2}+\frac{\partial^2 \psi^+}{\partial \theta^2}\right]$ and for the cold elliptic wall ($\eta=\eta_{NN}$=constant) we have:

$V_\eta^+ = V_\theta^+ = \frac{\partial \psi^+}{\partial \theta} = \frac{\partial \psi^+}{\partial \eta} = 0$, $T_2^+ = 0$ and

$\omega^+=-\frac{1}{H^2}\left[\frac{\partial^2 \psi^+}{\partial \eta^2}+\frac{\partial^2 \psi^+}{\partial \theta^2}\right]$. For the two diametrical plans ($\theta = \theta_1$= constant and $\theta = \theta_{NN}$=constant) we have:

$V_\eta^+ = V_\theta^+ = \frac{\partial \psi^+}{\partial \theta} = \frac{\partial \psi^+}{\partial \eta} = 0$, $\frac{\partial T^+}{\partial \theta}=0$ and

$$\omega^+=-\frac{1}{H^2}\left[\frac{\partial^2 \psi^+}{\partial \eta^2}+\frac{\partial^2 \psi^+}{\partial \theta^2}\right]$$

Once the temperature distribution is obtained; local Nusselt number value is given by the following relation:

$$Nu=-\frac{1}{H}\frac{\partial T^+}{\partial \eta}\bigg|_{\eta=cste} \qquad (14)$$

The average Nusselt number is expressed by:

$$\overline{Nu}=\frac{1}{\theta_{NN}-\theta_1}\int_{\theta_1}^{\theta_{NN}} Nu\,d\theta \qquad (15)$$

2. 1 Numerical Formulation

To solve the system of equations (11), (12) and boundary conditions, we consider a numerical solution by the finite volumes method. Where as for the equation (13), we consider a numerical solution by the centered differences method.

Both methods are widely used in the numerical solution of transfer problems; they are well exposed by Patankar (1980) and by Nogotov (1978). Figure 2 represents the physical and computational domain.

We cut out annular space according to the directions η and θ from the whole of elementary volumes or "control volume" equal to "$H^2.\Delta\eta.\Delta\theta.1$". (The problem is two-dimensional, the thickness in Z direction is assumed to the unity).

The center of a typical control volume is a point P and center of its side faces "east", "west", "north" and "south", are indicated respectively, by the letters e, w, n and s. Four other control volumes surround each interior control volume. The centers of these volumes are points E, W, N and S. the scalar variables (vorticity, temperature) are stored at centered points in control volumes. Thus transfer equations of scalar variables are integrated in typical control volume.

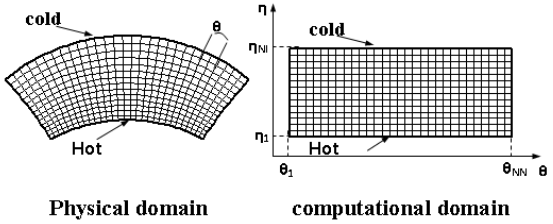

FIG. 2 Physical and computational domain

Figure 3 represents a typical control volume and its neighbors in a computational domain.

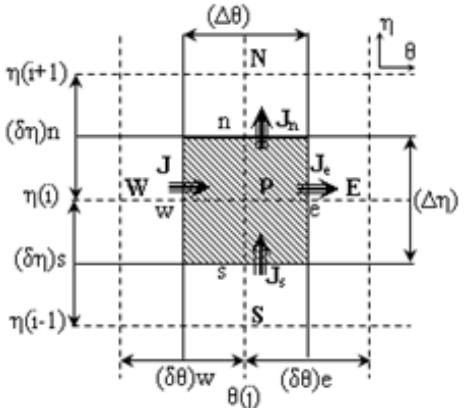

FIG. 3 A typical control volume and its neighbors in a computational domain

2. 2 Discretization of the general transfer equation of a variable φ in the control volume:

To illustrate the discretization of the transfer equations by finite volumes method, we consider the transfer equation in its general form:

$$\frac{\partial}{\partial \eta}\left(\mathrm{H}V_\eta^+\varphi-\Gamma_\varphi\frac{\partial \varphi}{\partial \eta}\right)+\frac{\partial}{\partial \theta}\left(\mathrm{H}V_\theta^+\varphi-\Gamma_\varphi\frac{\partial \varphi}{\partial \theta}\right)=S\varphi \qquad (16)$$

Sources and diffusion coefficients are specified in table 1.

Tab. 1 sources and diffusion coefficients of the variables φ

φ	Γ_φ	S_φ
T^+	1/Pr	0
ω^+	1	$\frac{Gr}{h}\left\{\begin{array}{l}[F(\eta,\theta)\cos(\alpha)-\mathrm{G}(\eta,\theta)\sin(\alpha)]\frac{\partial T^+}{\partial \eta}\\ -[F(\eta,\theta)\sin(\alpha)+\mathrm{G}(\eta,\theta)\cos(\alpha)]\frac{\partial T^+}{\partial \theta}\end{array}\right\}$

The discretization equation is obtained by integrating the conservation equations over the control volume shown in Figure 3 Patankar (1980), we obtain the following final form:

$$a_P \phi_P = a_N \phi_N + a_S \phi_S + a_E \phi_E + a_W \phi_W + b \qquad (17)$$

The coefficients of equation 17 are well defined by Patankar (1980), the Power Law scheme used to discretize the convectif terms in the governing equations.

3. RESULTS AND DISCUSSION

We consider two configurations for our cavity characterized by two values of inclination angle (0° and 45°) and a geometrical form factor (Fr = 5) which is defined by:

$$Fr = \frac{\eta_{NI} - \eta_1}{\theta_{NN} - \theta_1}$$

3.1 Grid study:

Several grids were used arbitrarily for the following configuration: (α=0° and Fr=1, for $Gr=10^3$, $Gr=10^4$ and $Gr=5.10^4$), to see their effect on the results, table 2 shows us the variation of average Nusselt number and the maximum of the stream function value according to the number of nodes for each grid. We choose the grid (101x111).

Tab. 2 Variation of average Nusselt number and the maximum of the stream-function value according to the number of nodes

	Gr =10^3		**Gr =10^4**		**Gr =5.10^4**	
$\eta_{NI}x\theta_{NN}$	ψ_{max}	$NU_{moy.}$	ψ_{max}	$NU_{moy.}$	ψ_{max}	$NU_{moy.}$
41x51	0.090	1.387	5.582	2.689	16.575	4.268
51x61	0.090	1.387	5.588	2.685	16.572	4.234
61x71	0.109	1.387	5.593	2.682	16.566	4.197
71x81	0.130	1.387	5.596	2.680	15.560	4.197
81x91	0.179	1.387	5.596	2.678	15.555	4.195
91x101	0.201	1.387	5.596	2.678	15.549	4.190
101x111	0.219	1.389	5.596	2.674	15.549	4.190
111x121	0.219	1.389	5.596	2.674	15.549	4.190

3.2 Numerical code validation

Kuehn et al. (1976) have developed a numerical study on natural convection in the annulus between two concentric and horizontal cylinders with a radius was taken equal to 2.6, they calculated a local equivalent thermal conductivity, defined as being the report of a temperature gradient in a convective and conductive heat exchange on a temperature gradient in an exchange conduction:

$$\lambda_{éq} = \frac{\left.\frac{\partial T^+}{\partial \eta}\right|_{convection+conduction}}{\left.\frac{\partial T^+}{\partial \eta}\right|_{conduction}}$$

They calculated an average value of the conductivity. To validate our numerical code, we compared the average value derived from our calculations with their results. Table 3 illustrates this comparison and we find that quantitatively our results and theirs are in good agreement.

Tab. 3 Comparison of the average thermal conductivity of Kuehn with our results

	Pr	0,70	0,70	0,70	0,70
	Ra	10^2	10^3	$6x10^3$	10^4
Inner wall	Kuehn	1,000	1,081	1,736	2,010
	Presents calculs	1,000	1,066	1,730	2,068
	|E(%)|	**0,000**	**1,388**	**0,346**	**2,886**
Outer wall	Kuehn	1,002	1,084	1,735	2,005
	Presents calculs	1,002	1,066	1,736	2,078
	|E(%)|	**0,000**	**1,661**	**0,058**	**3,641**

3.3 Influence of the Grashof number

3.4 Isotherms and streamlines

Figure 4 and figure 5 represent the isotherms and the streamlines for different values of the Grashof number when α=0°.

We note that these isotherms and these streamlines are symmetrical about the median fictitious vertical plane. These figures show that the structure of the flow is bi-cellular. The flow turns in the trigonometrically direction in the left side and in opposite direction in the right one (the fluid particles move upwards along the hot wall).

For $Gr=10^2$ the isotherms are almost parallel and concentric curves which coincide well with active walls profiles. In this case the temperature distribution is simply decreasing from the hot wall to the cold wall. The streamlines of the fluid show that the flow is organized in two cells that rotate very slowly in opposite directions.

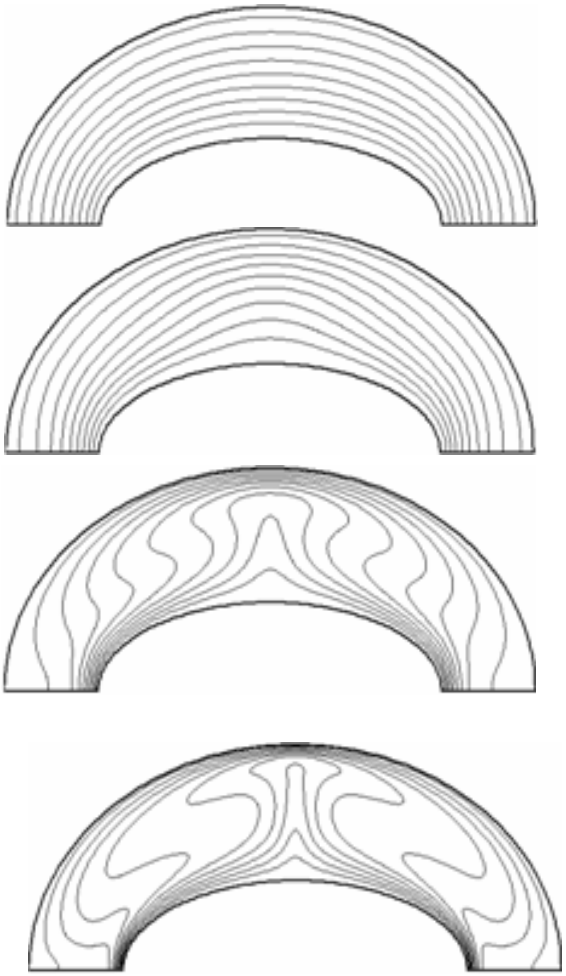

FIG. 4 Isotherms for e_1=0.86, Fr=5, α=0° and respectively Gr=10^2, Gr=10^3, Gr=10^4 and Gr=5.10^4

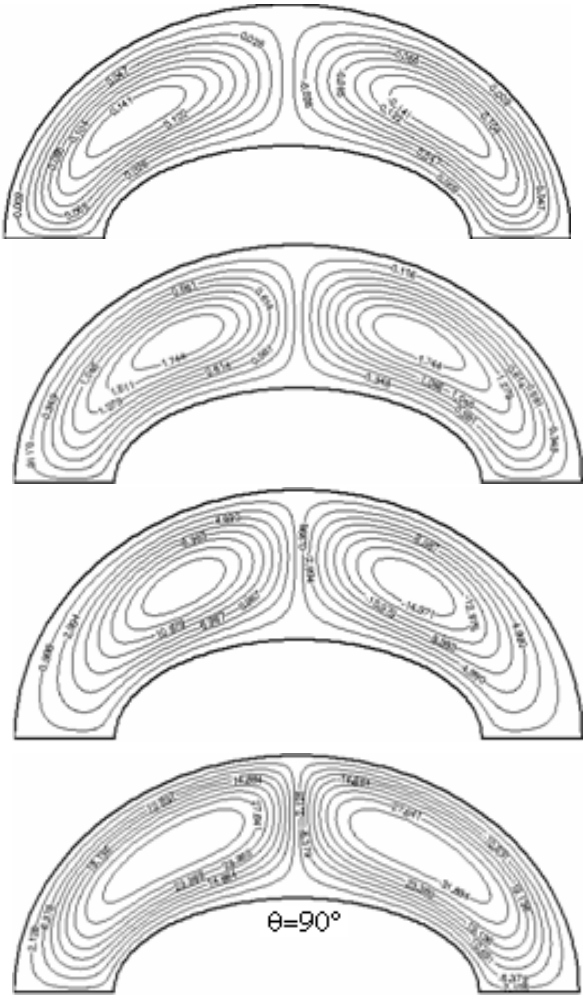

FIG. 5 Streamlines for e_1=0.86, Fr=5, α=0° and respectively Gr=10^2, Gr=10^3, Gr=10^4 and Gr=5.10^4

We can say that the heat transfer is mainly conductive. The values of the streamline which are given on the corresponding figure are very small.

For Gr=10^3 the isothermal lines are transformed symmetrically with respect to the vertical axis and change significantly, and the values of the streamlines mentioned on the same figure, increase also significantly, which translates a transformation of the conductive transfer to the convective transfer, but relatively low as shown in the isotherms shape.

However for Gr=10^4 the isotherms are modified and eventually take the form of a mushroom. The temperature distribution decreases from the hot wall to the cold wall. The direction of the deformation of the isotherms is consistent with the direction of rotation of the streamlines. In laminar flow, we can say that under the action of the particles movement taking off from the hot wall at the symmetry axis, the isotherms move away from the wall there. The values of the stream functions increase which means that the convection intensifies.

The increase of the Grashof number to 5.10^4 intensifies the convection as shown in corresponding figures.
Let us note that the isotherms, of all the figures indicated above, were plotted with a ΔT^+=0.1

3.5 Local Nusselt Number

We determine the local Nusselt numbers for which changes along the walls are closely related to the distributions of isotherms and streamlines, so that, qualitatively, these variations and distributions can often be deduced from each other. For example, if we consider a current point on a wall following a coordinated observation of a monotonous reduction in the local Nusselt number corresponds to a directed flow following this coordinate, the observation of an increase corresponds to a directed flow in opposite direction.

3.6 Analogy between the variation of local Nusselt number -isotherms and streamlines

We thus notice on Figure 6, that the variations of local Nusselt number on the inner activate wall are in accordance

with what has just been indicated above, a minimum reflects an existence of two counter-rotating cells pushing away the fluid from the wall, a maximum reflected, on the contrary, the existence of two counter-rotating cells providing the fluid to the wall. What thus enables us to follow the evolution of our flow in our annular space.

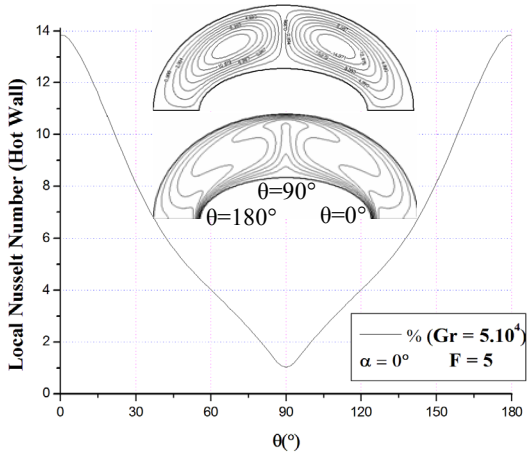

FIG. 6 Variation of local Nusselt number on the inner activate wall

3.7 Variation of local Nusselt number on the hot wall

Figure 7 illustrates the variation of local Nusselt number on the hot wall, and allows us to notice that with the increase of the Grashof number, the value of local Nusselt number on this wall also increases, which is obvious.

3.8 Effect of the angle of inclination α :

We examine here the effect of the inclination of the system compared to the horizontal plane, the angle α is measured from the horizontal plane in the trigonometric direction. We used two values of α (0° and 45°).

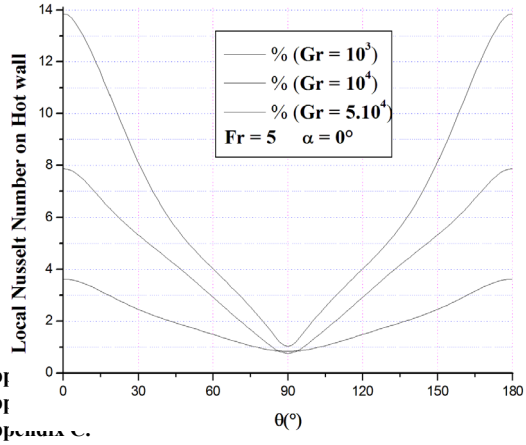

Appendix C.

FIG. 7 Variation of local Nusselt number on the hot wall

Appendix D.

3.9 Case where the inclination angle α is zero

In this case, the vertical fictitious median plane is in principle a symmetry plane for transfer phenomena. Therefore by symmetry and in relation to this vertical plane depending on the value of Grashof number, the flow is organized always in two principal cells rotating in opposite directions, as the figures (4-5) show.

3.10 Case where the inclination angle α = 45°

When α=45°, the symmetry of the system relative to the fictitious vertical plane is destroyed as well illustrated in figure 8 and figure 9, the ends of annular space move upwards for the right part of the system and downwards for the left part. Figure 9 show that the cell of left can more develop that its counterpart on the right part and tends to occupy the entire annular space as the system is inclined more until becoming vertical.

3.11 Local and average Nusselt number

The figure 10 which illustrates the variation of local Nusselt number on the hot wall shows that for α=0° the minimum of local Nusselt number is reached at the angular position θ=90°, which is in agreement with figure 5 which shows that the two cells meet at this precise place while moving away the fluid from this wall. For α=45° the minimum of local Nusselt number moves at the position θ=53°, which is in agreement also with figure 9 which shows that for this inclination, the two cells meet at this angular position while moving away the fluid there from this wall.

FIG. 8 Isotherms for e_1=0.86, Fr=5, α=45° and Gr=5.10^4

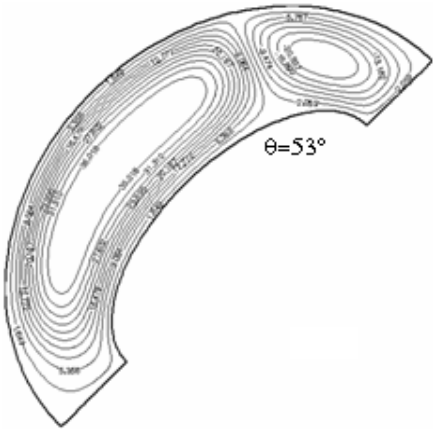

FIG. 9 Streamlines for e_1=0.86, Fr=5, α=45° and Gr=5.10^4

The variation of average Nusselt number on the hot wall as a function of Grashof number illustrated in figure 11 which shows that the inclination α is then without influence when Gr≤10^3, this translates that the heat transfer is primarily conductive. For the greatest values of the Grashof number, α influences the convective transfer.

CONCLUSION

We established a mathematical model representing the transfer of movement within the fluid and heat through the active walls of the enclosure. This model based on the assumption of Boussinesq and the bidimensionnality of the flow. We have developed a calculation code, based on the finite volume method, which determines the thermal and dynamic fields in the fluid and the dimensionless numbers of local and average Nusselt on the active walls of the enclosure, depending to the quantities characterizing the state of the system. The influence of the Grashof number and the inclination of the system, on the flow in stationary mode has been particularly examined.

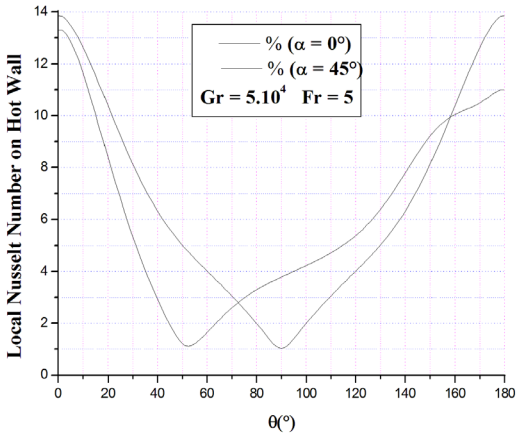

FIG. 10 Variation of local Nusselt number on the hot wall

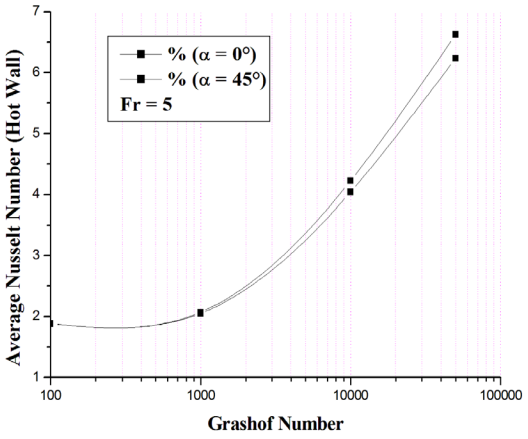

FIG. 11 Variation of the average Nusselt number on the inner activate wall

Appendix E.
Appendix F.
Appendix G.
Appendix H.
Appendix I.
Appendix J.
Appendix K.
Appendix L.
Appendix M.
Appendix N.
Appendix O.
Appendix P.
Appendix Q.

The results of the numerical simulations have shown that conduction is the regime of heat transfer dominant for Grashof numbers lower than 10^3. For Grashof numbers higher than 10^3, the role of the convection becomes dominant, this on the one hand, on the other hand we saw that the transfers are better when our system presents elements of symmetry.
Appendix R.

REFERENCES

[1] T.H.Kuehn, R.J. Goldstein, An experimental and theoretical study of natural convection in the annulus between horizontal cylinders, J. Fluid Mech., 74, 695-719, 1976.

[2] Y.D.Zhu, C. Shu, J. Qiu, J. Tani,Numerical Simulation of natural convection between two elliptical cylinders using DQ method, Int. J. Heat. Mass. Trans., 47, 797-808, 2004.

[3] M.Djezzar,M. Daguenet, Numerical study of bidimensional steady natural convection in a space annulus between two elliptic confocal ducts. 1ST International Conference on Thermal Engineering Theory and Applications. Beïrut-Lebanon, du 31 Mai au 04 Juin, 2004.

[4] M.Djezzar,M. Daguenet, Contribution to the study of the convection in various annular spaces, subjected to various conditions of heating. Thesis of Doctorate of state, University Mentouri Constantine, 2005.

[5] M.Djezzar,A. Chaker,M. Daguenet, Numerical study of bidimensional steady natural convection in a space annulus between two elliptic confocal ducts: Influence

of internal eccentricity. Revue des Energies Renouvelables. 8, 63-72, 2005.

[6] M.Djezzar,M. Daguenet, Natural steady convection in a space annulus between two elliptic confocal ducts: Influence of the slope angle. Journal of Applied Mechanics Transaction of the ASME, 72, 88-95, 2006.

[7] S.V.patankar , Numerical Heat Transfer and fluid flow, (McGraw-Hill book company), ppc113-137. New York,1980.

[8] P.Moon, E. Spencer, Field theory Engineers, (D. VAN. Nostrand company), p 356. LTD, Torronto,, Canada , 1961.

[9] E.F.Nogotov, Applications of Numerical Heat Transfer, (McGraw-Hill book company), ppc122-125. New York, 1978.